PROCEEDINGS, 43rd Workshop on Geothermal Reservoir Engineering
Stanford University, Stanford, California, February 12-14, 2018
SGP-TR-213

CFD modeling of a high enthalpy geothermal context

Theo Renaud, Michal Stebel[1], Patrick Verdin, Gioia Falcone

Geo-Energy Engineering Centre, Cranfield University, MK43 0AL, UK

theo.renaud@cranfield.ac.uk

Keywords: CFD, IDDP, geothermal, reservoir.

ABSTRACT

The promising development of highly energetic geothermal resources could considerably enhance geothermal power production worldwide. The first attempt at tapping supercritical/heated fluids was made by the Iceland Deep Drilling project (IDDP), but unfortunately a magma layer at a depth of 2,100m was encountered, and the drilling was abandoned. Yet, this drilling operation failure generated new opportunities for assessing the potential power generation close to shallow magmatic intrusions. Detailed numerical methods are required to assess the heat transfer and fluid thermodynamics at wellbore and reservoir scale at near supercritical conditions to provide production scenarios and forecasts as accurate as possible. A primary steady-state study of reservoir and wellbore heat extraction from a geothermal well near a magmatic chamber has been performed with Computational Fluid Dynamics (CFD) techniques. Using simplified geological assumptions based on the IDDP-1 well description, a 2D axisymmetric single phase flow model was developed and its results were compared to those obtained with a full 3D CFD model. The simulated output power simulations reached 25 MW at 350°C and a wellhead pressure of 140 bars. Methodology and results from this study show that CFD techniques can be successfully used to assess geothermal energy outputs for unconventional geothermal wells and can provide details of a vapor superheated flow structure at wellbore-reservoir scale.

1. INTRODUCTION

The need for sustainable energy supplies raises thrilling challenges to develop low-carbon emitting technologies and decrease dependency on fossil fuels (Fuss et al., 2008). Geothermal energy already contributes to generate power and heat worldwide, reaching a total electric capacity of 10.9 GW in 24 countries; this is expecting to increase in the future (Bertani, 2012).

In 2009, the drilling into very high enthalpy geothermal resources in Iceland raised new opportunities for increasing the potential power generation per well (Elders et al., 2014). More recently, on the 25 January 2017, the second well of the Iceland Deep Drilling Project (IDDP-2) successfully reached 427°C and a fluid pressure of 34 MPa at a depth of more than 4,500 m. At such thermodynamics conditions above the critical point of pure water (22 MPa, 374°C), the enthalpy increases sharply, the density decreases and the energy available per unit of volume is 20 times higher than with conventional extracted geothermal fluids (Suarez Arriaga and Samaniego 2013). During the initial test in 2010, superheated steam was recovered from circulating water heated by a permeable rock above the magma intrusion (Axelsson et al., 2014). The modeling of the fluid properties near the bottom of the well showed an enthalpy of 2,900 kJ/kg at 160 bars and 390°C. In the initial phase of the project, the well IDDP-1 produced 10-12 kg/s of dry superheated steam (Friðleifsson et al., 2014). The measured temperature reached 440°C at the surface with a well pressure around 150 bar (Ingason et al., 2014). This was stopped at a depth of 2,072 m as a magma layer was encountered somewhere between 2,092 m and 2,104 m (Pálsson et al., 2014).

Numerical codes can be used to assess supercritical fluid flow and heat transfer in porous media. Examples include HYDROTHERM (Hayba and Ingebritsen 1994), HOTH2O extension of STAR (Pritchett, 1995) and the TOUGH2 code (Kissling, 1995; Brikowski, 2001) extended with AUTOUGH2 (Croucher and O'Sullivan 2008) and an inverse modelling module iTOUGH2 (Magnusdottir and Finsterle 2015). In addition, a modified extension of the SHEMAT-Suite code was applied to simulate supercritical conditions in a two-phase water/steam reservoir in Tuscany (Büsing et al., 2016) and the Complex System Modelling Platform CSMP++ (Weis et al., 2014) was able to model supercritical conditions near magmatic intrusions with complex geometries (Scott et al., 2015a).

Although these simulators are well-established tools for modeling supercritical fluid flow and heat transfer in porous and fractured media, they do not deal with the processes occurring near the bottom hole and along the wellbore. Even if the T2Well code (Pan et al., 2015) calculates a wellbore numerical solution for a Water - NonCondensibleGas - NaCL equilibrium (Vasini, 2016), it is limited in temperature and pressure for supercritical issues (350°C and 1000 bars), especially for the conditions observed in the IDDP project.

Numerical studies on closed well systems are documented in the literature (Lenhard and Malcho 2013; Huang et al. 2015). Only a limited number of CFD based studies have however been performed and are reported for geothermal reservoir management with open wells. One such study describes a homogeneous 3D Enhanced Geothermal System (EGS) run with the steady-state (Chen and Jiang, 2015) and the transient solvers to consider thermal non-equilibrium conditions between solid and fluid (Jiang et al., 2013).

[1] Now with the Silesian University of Technology, Poland

The modeling of supercritical fluid heat transfer using CFD techniques is mainly limited to nuclear engineering applications involving water (Cheng et al., 2007). For supercritical CO_2, a doublet fractured EGS was investigated using the NIST real gas model formulation in the commercial code ANSYS Fluent (Fluent 2016), which provides supercritical thermodynamics properties (Luo et al., 2014; Jiang et al., 2017). Cheng et al. (2007) established that the choice of turbulence model (k-ω in this case) can produce inaccurate results at supercritical pressure. However, their model showed reasonable predictions of Heat Transfer Coefficient and wall temperature. Recently, the wellbore heat transfer was investigated considering constant water properties using a k-ε turbulence model (Huang et al. 2015a, Huang et al. 2015b). From the latter study, the heat in the production well was transferred to the surroundings and a steady heat transfer process could be considered after 30 days.

In the work described here, the steady state heat transfer and fluid flow processes in a geothermal well and a porous medium are investigated numerically with the CFD code ANSYS Fluent 17.1.0. Geometry and data from the IDDP-1 well are used to create the model and apply boundary conditions. CFD-based predicted results are analysed to obtain surface and bottom hole data, for different magma temperatures and production mass flow rates. Two different turbulence models are tested in the wellbore and laminar flow conditions are applied in the porous medium. Results obtained with a 2D axisymmetric model are compared to those obtained with a full 3D model.

2. METHODOLOGY

2.1 Model description

The geometry and the mesh were created with the pre-processor ICEM CFD 17.1.0. For the model development phase and to obtain results quickly, a 2D axisymmetric model was considered first, see **Figure 1**. The domain investigated contains a 80 m radius saturated porous zone delimited by the ground surface (x=0 m) up to x=- 2,100 m (Zone 1). A simplified geothermal well is present, from x=0 m up to x=-2070 m. The wall of this well is represented by the plain black line on **Figure 1**. To keep a mass equilibrium and to allow a mass flow inlet boundary condition to be applied far away from the well, the domain is extended from 80 m to 100 m in the radial direction r, between x=-2,000 m and x=-2,100 m (Zone 2) and is terminated by a wall. It is assumed that no exchange is present on this wall, although this is clearly not the case in reality. However, this assumption is valid as the wall is located far away from the well, so will not have any effect on the flow in that region. As a first assumption, the well is described as an open well with same properties and diameter as the slotted liner (9-5/8" -240 mm) present in the IDDP-1 project (Ingason et al., 2014). Thus, the producing zone is only limited at a depth of 2,070 m, and not from potential upper zones as raised by Pálsson et al. 2014. A "Pressure outlet" boundary condition is applied at the well exit (x=0 m). A 10 m thick unsaturated conductive layer separates the porous zone (Zone 2) from the magma region located at a depth of 2,100 m (Zone 3). A structured mesh was generated, comprising 1,400,760 cells, with local refinements present inside and around the wellbore.

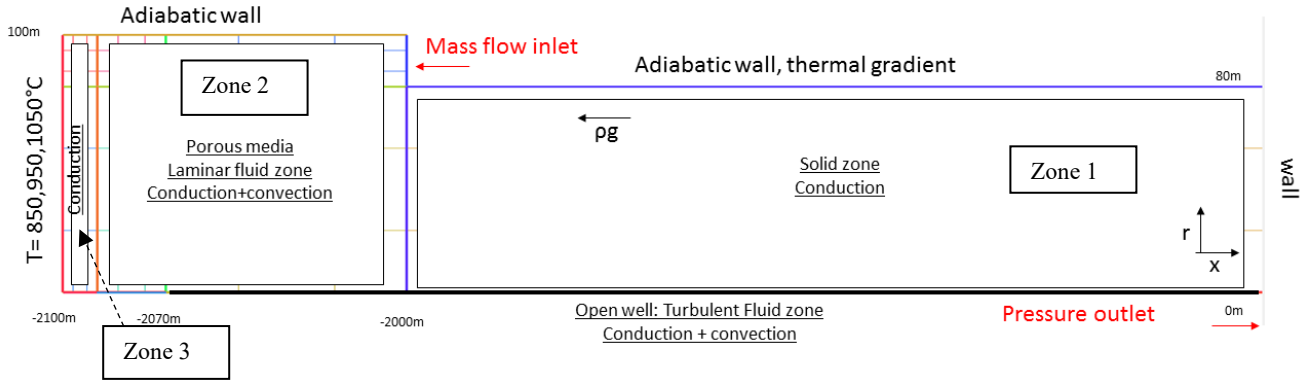

Figure 1: Schematic representation of the axisymmetric model

The porous media properties are taken from Axelsson et al. (2014) and the well properties from Duan et al. (2016). The porous media porosity is set to 10% (Axelsson et al., 2014) with a homogeneous permeability of 10^{-14} m² (Scott et al., 2015b). If not specified, the magma layer temperature is set by default to 850°C (Elders et al., 2011). The density, specific heat and thermal conductivity of the porous media are set to 2,700 kg/m³, 800 J/kg.K and 1.5 W/m.K, respectively. For the well, the following material properties are considered: 7,848 kg/m³, 460 J/kg.K. To account for the cement which surrounds the casing up to x=-1950 m (Pálsson et al., 2014), the wellbore material is set to 0.3 W/m.K for Portland Cement (Thórhallsson et al., 2014) rather than considering the casing properties (45.65 W/m.K). The wellbore considered is 15 mm thick. The injected fluid is water vapor; its density ρ is calculated with the ideal gas law:

$$p = \rho.R.T \tag{1}$$

where p and T are the static pressure (Pa) and temperature (K) respectively. R is the gas constant equal to 8.314 $J.K^{-1}$ mol^{-1}.

The wellhead pressure outlet is set to 140 bars. The vapor properties (specific heat, thermal conductivity, viscosity) are implemented via a temperature linear approximation based on a 160 bar constant pressure, see the **Appendix** section for details. User defined functions (UDFs) have been created to apply a local geothermal gradient on the side of the model, based on the temperature measurements along the IDDP-1 well (Axelsson et al., 2014; Mortensen et al., 2014).

A full 3D model was also created with a structured mesh composed of 2,918,202 cells. The system investigated is identical to the 2D axisymmetric one, but a conventional rectangular domain considered in CFD geothermal modeling (Huang et al., 2017) was used to run the numerical simulations.

2.2 Mathematical model

The governing equations are solved with the CFD code ANSYS Fluent 17.1.0, which is based on the finite volume approximation. The flow in the porous medium is considered as laminar while a turbulent model is applied in the well. For an axisymmetric model, the continuity equation is written as:

$$\frac{\partial \rho}{\partial t}+\frac{\partial(\rho v_x)}{\partial x}+\frac{\partial(\rho v_r)}{\partial r}+\frac{\rho v_r}{\partial r}=0 \tag{2}$$

2.1.1 Laminar model

The momentum equations in the porous medium are defined for a laminar flow with the following equations:

$$\frac{\partial(\rho v_x)}{\partial t}+\frac{1}{r}\frac{\partial(r\rho v_x v_x)}{\partial x}+\frac{1}{r}\frac{\partial(r\rho v_r v_x)}{\partial r}=-\frac{\partial \rho}{\partial x}+\frac{1}{r}\frac{\partial[r\mu(2\frac{\partial v_x}{\partial x})-\frac{2}{3}(\nabla.\vec{v})]}{\partial x}+\frac{1}{r}\frac{\partial[r\mu\frac{\partial v_x}{\partial r}+\frac{\partial v_r}{\partial x}]}{\partial r}+\rho\vec{g} \tag{3}$$

$$\frac{\partial(\rho v_r)}{\partial t}+\frac{1}{r}\frac{\partial(r\rho v_x v_r)}{\partial x}+\frac{1}{r}\frac{\partial(r\rho v_r v_r)}{\partial r}=-\frac{\partial \rho}{\partial r}+\frac{1}{r}\frac{\partial[r\mu(\frac{\partial v_r}{\partial x}+\frac{\partial v_x}{\partial r})]}{\partial x}+\frac{1}{r}\frac{\partial[r\mu(2\frac{\partial v_r}{\partial r}-\frac{2}{3}(\nabla.\vec{v})]}{\partial r}$$
$$-2\mu\frac{v_r}{r}+\frac{2}{3}\frac{\mu}{r}(\nabla.\vec{v}) \tag{4}$$

$$\text{where } \nabla.\vec{v}=\frac{\partial v}{\partial x}+\frac{\partial r}{\partial r}+\frac{v_r}{r} \quad \text{, with } v \text{ the fluid velocity and } \mu \text{ its molecular viscosity.} \tag{5}$$

The energy equations in the fluid and solid zone are:

$$\frac{\partial(\rho E)}{\partial t}+\nabla.(\vec{v}(\rho E+p))=\nabla.(k_{eff}\nabla T-\sum_j h_j\vec{J}_j+(\overline{\overline{\tau_{eff}}}.\vec{v})) \qquad \frac{\partial(\rho h)}{\partial t}-k\nabla T=0 \tag{6) and (7}$$

k_{eff} is the effective thermal conductivity $k+k_t$, with the turbulence thermal conductivity k_t equals to 0 in the laminar zone. The stress tensor τ_{eff} is defined and can be retrieved in the Fluent User Guide (Fluent 2016). The energy *E* and the sensible enthalpy *h* are calculated via Equations (8) and (9):

$$E=h-\frac{p}{\rho}+\frac{v^2}{2} \qquad h=\int_T^{T_{ref}} cdT+\frac{p}{\rho}, \quad \text{where } c \text{ is the heat capacity} \tag{8) and (9}$$

2.1.2 Turbulence model

As a high fluid velocity and the Reynolds number in the well are expected to be high, turbulence is considered. Two models are investigated: the standard k- ε and the k-ω SST (Menter, 1993). The standard turbulence k-ε model is based on transport equations for the turbulence kinetic energy (k) and its dissipation rate (ε) (Fluent 2016). This model is fast and has proved to be efficient at high speed and suitable for numerous industrial applications. The k-ω Shear Stress Transport (SST) turbulence model calculates the turbulent kinetic energy and the specific dissipation by modification of the turbulent viscosity formulation to account for the transport effects of the principal turbulent shear stress. Continuum equations can be written as:

$$\frac{\partial(\rho k)}{\partial t}+\frac{\partial(\rho k v_i)}{\partial x_i}=\frac{\partial}{\partial x_j}(A_k\frac{\partial k}{\partial x_j})+B \qquad \frac{\partial(\rho C)}{\partial t}+\frac{\partial(\rho C v_i)}{\partial x_i}=\frac{\partial}{\partial x_j}(A_{\varepsilon,\omega}\frac{\partial k}{\partial x_j})+S \tag{10) and (11}$$

The effective diffusivity $A_{k,\varepsilon,\omega} = \mu + \frac{\mu_t}{\sigma_{k,\varepsilon,\omega}}$ with $\sigma_{k,\varepsilon,\omega}$ the turbulent Prandtl number and the eddy viscosity μ_t are described in Fluent 2016.

The SST formulation combines: (i) the use of a k–ω formulation in the inner parts of the boundary layer which makes this model directly usable in the viscous sub-layer and can therefore be used as a Low-Re turbulence model , and (ii) a switch to a k–ε model in the bulk flow and therefore avoids sensitivity problems encountered by a k–ω formulation due to inlet turbulence properties (Fluent 2016). The different terms present in the continuum equation for both models are reported in **Table 1**.

Table 1: Terms in continuum equation

Turbulence model	$A_{\varepsilon,\omega}$	B	C	S
k-ε	A_ε	$G_k + G_b - \rho\varepsilon - Y_M$	ε	$C_{1\varepsilon}\frac{\varepsilon}{k}(G_k + C_{3\varepsilon}G_b) - C_{2\varepsilon}\rho\frac{\varepsilon^2}{k}$
k-ω	A_ω	$G_k - Y_M$	ω	$G_\omega - Y_\omega + D_\omega$

G_k, G_b represent respectively the generation of turbulent kinetic energy due to mean velocity and buoyancy. They are defined with Y_M (dilatation in compressible turbulence), D_M (cross-diffusion term) and the constants $C_{1,2,3,\varepsilon}$ in Fluent 2016.

2.1.2 Numerical model

For all CFD simulations described here, the SIMPLE (Semi-Implicit Method for Pressure Linked Equation) algorithm was used to address the pressure-velocity coupling. A first order upwind differencing scheme was applied for the discretization of the spatial-derivative terms. Energy, density, turbulence, momentum and the specific dissipation rate component were all based on a first order upwind scheme. The standard method was chosen for the pressure solution. The steady solver was applied and gravity effects were considered. A convergence criterion of 1e-03 was set-up for every equation apart from the energy, where a value of 1e-6 was applied.

3 RESULTS AND DISCUSSION

3.1 Ideal gas modeling

Figure 2a shows a 2D contour plot of the temperature distribution in the whole domain and a closer view near the bottom hole of the well, when the k-ε turbulence model is used with a water vapor injection of 30kg/s. As can be seen, the temperature is very high in the magma region and decreases axially as the distance from this region increases. In the bottom hole zone, a temperature of 430°C is reached and propagates into the well. **Figure 2b** describes the numerical results of temperature along the centerline of the well when considering water vapor injections of 1kg/s, 10kg/s and 30kg/s, the k-ε and the k- ω turbulence models, and different magma temperatures: 850°C (the default temperature), 950°C and 1050°C.

At the bottom hole, the vapor temperature rises locally in the well due to the pressure drop between the porous medium and the well zone. When a mass flow rate of 10-30kg/s is applied at the inlet, the wellhead temperature reaches 358°C ± 10°C with maximum depth variations evaluated around 5 %. The 1kg/s case drives more heat, but the vapor shows significant thermal losses with the surrounding rocks toward the surface. A 3 % variation in results is noted between the k-ε and k-ω turbulence models in the wellbore region.

A slightly higher wellhead temperature is observed when increasing the magma temperature, while the temperature distribution in the porous medium is highly affected (**Figure 2b**). Note that in this region, a 850°C threshold appears due to calculation limitations in the ideal gas formulation.

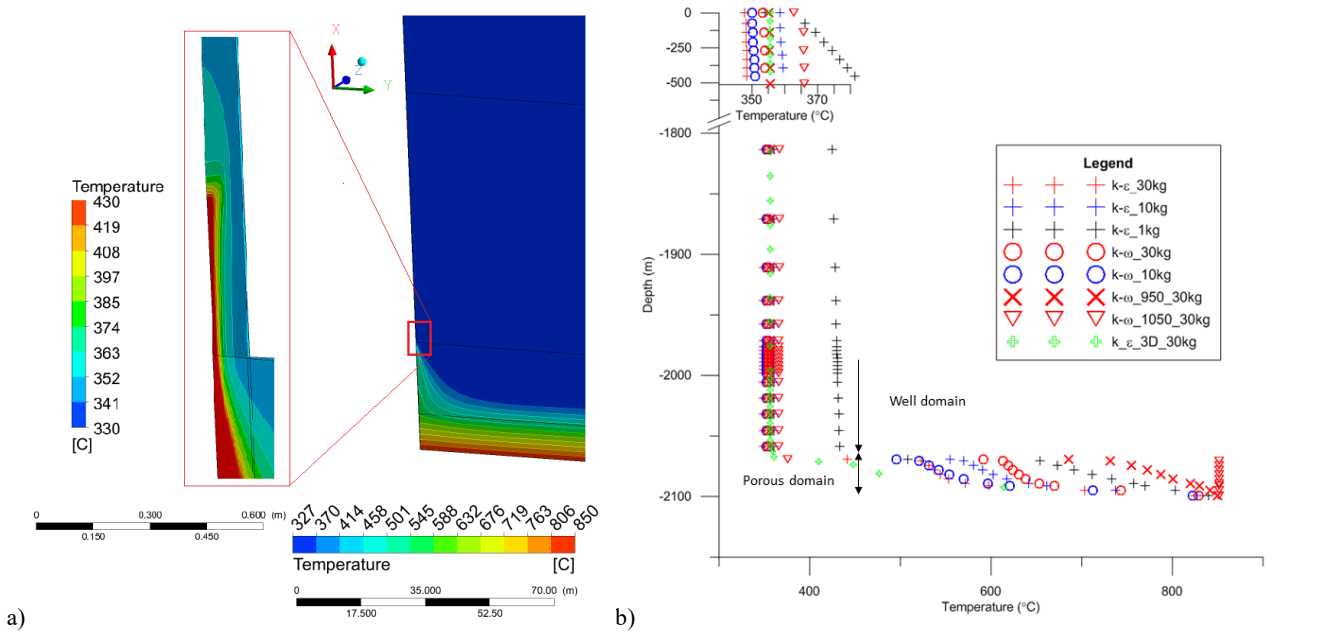

Figure 2: a) Temperature distribution of the near bottom hole area (left) and below 2,000 m (right) for the k-ε_30kg simulation. b) Temperature distribution along the centerline (x=0 m).

3.2 3D vs axisymmetric modeling

Figure 3a shows the temperature distribution in the direction normal to the well axis at x=-1000 m, where the flow is fully developed, from the center of the well (r=0m) to the radius r=1 m. **Figure 3b** summarizes the fluid velocity, density, enthalpy and output power when the magma temperature is 850°C with the k-ε and k–ω turbulence models for different injection mass flow rates. 2D axisymmetric and full 3D based results are compared on **Figure 3a**. Only the k-ε turbulence model was investigated in the 3D model, as it has been seen previously for the 2D axisymmetric study that the difference of results between the two turbulence models tested is small, around 5°C. The 3D simulation provides results slightly hotter than those obtained with the axisymmetric case, but reasonably consistent when looking at the range of output temperature values. An axisymmetric model can therefore be used instead of a full 3D model for such studies, which reduces computational costs significantly.

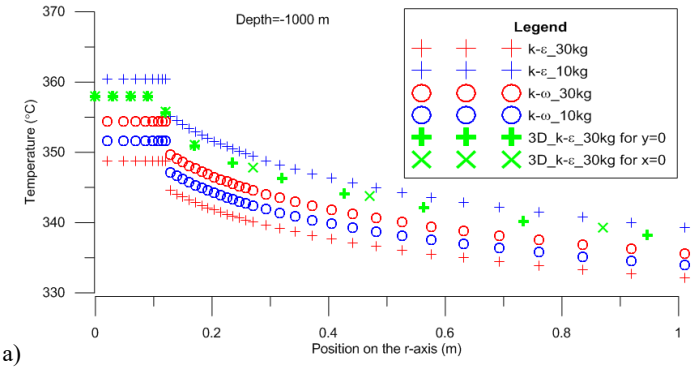

b)

Magma Temp=850°C	k- ε		k-ω SST
	30kg	10kg	30 kg
Velocity (m/s)	14.81	5.02	14.98
Density (kg/m³)	49.19	48.40	48.74
Enthalpy (kJ/kg)	2731.13	2804.60	2773.26
Potential output power (MW)	24.58	8.41	24.95

Figure 3: a) Radius temperature distribution at 1,000m between the axis center of the well and 1 m in the surroundings rocks. The 3D results are shown for two orthogonal horizontal directions (x, y). b) Simulation-based output results

Simulated results in the porous media zone obtained with the 2D axisymmetric and the 3D models are significantly different, see **Figure 2b**. In the first meters below the bottom hole, the axisymmetric simulation presents a sharp temperature drop while the 3D model shows a slower decreasing distribution. The comparative use of the k-ε and k-ω model gives very wide temperature upstream flow variations, which do not seem to follow any general rule.

In the wellbore, the bottom hole pressures reaches 14.9-15.3 MPa (around 150 bars). The mass flow rate applied leads to unrealistic values in the porous medium (1000-2000 bars). Thus, the properties calculated in the permeable zone are open to discussion. The model calculates a high Reynolds number value (Re>10,000) between -2070 m and -2069 m and rapidly reaches a constant value (100-500) indicating a

laminar flow behavior. Surprisingly, applying a hotter magma temperature does not affect the wellhead temperature. It seems that the output conditions constrain the model to converge at 358°C±10°C for 140 bars.

The applied ideal-gas formulation calculates correctly the vapor state above the saturated point of pure water (140 bar-336°C estimated from IAPWS-97 (Wagner et al., 2000)) but underestimates the gas density (around 50 kg/m³ while a value of 71 kg/m³ is estimated from IAPWS-97), see **Figure 3b**. Assuming a saturated vapor might not be correct for brine geothermal fluids as the boiling point curve of pure water and seawater diverge significantly above 300°C (Arnorsson et al., 2007). Considering a pessimistic net generation efficiency value of 30% (DiPippo, 2015), the potential output power simulated with an infinite source of heat provides almost 25 MW for 30 kg/s of steam flowing towards a dry steam plant (**Figure 3b**).

The simulations performed provide a steady state assessment with a constant magma temperature and geothermal fluids circulation. These assumptions imply that the geothermal system is continuously supplied, which may not be true at large time scale and during excessive production. The surface results are underestimated compared to the literature, but the bottom hole temperature values are in a similar range as those obtained through modeling by Axelsson et al. (2014). The differences of output results could be explained by the steady state formulation considered. Indeed, the production of superheated vapor during flow testing may be seen as a transient state regarding an initial reservoir state recently drilled. In addition, numerous assumptions were considered (boundary conditions, pure vapor, etc.). These might need revisiting and updating with potential in-situ properties.

5 CONCLUSION

A CFD modeling study of a very high enthalpy geothermal system including a simplified wellbore domain was performed. The heat transfer and fluid flow of an ideal-gas formulation for vapor were analyzed. The results show that both the 2D axisymmetric and the full 3D models generate close results in the wellbore. Because of its higher computational efficiency, the axisymmetric model can be considered suitable for the well and the surroundings rocks, but might not be accurate enough in the reservoir area. A decrease of the mass flow rate production drives more heat from the reservoir, but cools down faster when flowing up to the surface. The use of steady state conditions with a constant bottom layer temperature can assess a long-term power production.

CFD simulations can be useful for assessing new heat recovery methods in dedicated environment with an infinite source of heat regarding the surface facilities lifetime. However, it has been shown in this study that the water circulation simulated with a constant mass flow within the porous media needs to be investigated further. The number of assumptions should also be reduced to generate a more robust model, potentially with the inclusion of in-situ properties.

ACKNOWLEDGEMENT

The financial support from the UK Engineering and Physical Sciences Research Council (EPSRC) is grateful acknowledged. The authors also acknowledge Tomasz Cieszewski for his involvement in discussions related to this project.

APPENDIX

Temperature (K)	Specific Heat (J/kg.K)	Thermal Conductivity (W/m.K)	Viscosity (kg/m.s)
423 K	4266	0.6934	1.86E-04
473 K	4422	0.6749	1.38E-04
523 K	4732	0.6315	1.09E-04
573 K	5476	0.5587	8.83e-05
623 K	8789	0.1041	2.29e-05
673 K	4178	0.07994	2.5e-05
723 K	3269	0.07850	2.72e-05
773 K	2896	0.08138	2.94e-05
823 K	2711	0.08585	3.15e-05
873 K	2612	0.09113	3.35e-05
923 K	2557	0.09691	3.55e-05
973 K	2529	0.1030	3.75e-05
1023 K	2517	0.1094	3.94e-05
1073 K	2515	0.1160	4.13e-05

Appendix 1: Pure vapor thermal properties at 160 bars used in the piecewise linear function (Wagner and Krezschmar, 2010)

REFERENCES

ANSYS *Ansys Fluent Theory Guide*. (2016).

Arnorsson, S., Stefansson, A. and Bjarnason, J. O. Fluid-Fluid Interactions in Geothermal Systems, *Reviews in Mineralogy and Geochemistry*, 65, pp. 259–312. (2007).

Axelsson, G., Egilson, T. and Sif Gyldadóttir, S. Modelling of temperature conditions near the bottom of well IDDP-1 in Krafla , Northeast Iceland, *Geothermics*, 49, pp. 49–57. (2014).

Bertani, R. Geothermal power generation in the world 2005-2010 update report, *Geothermics*, 41, pp. 1–29. (2012).

Brikowski, T. H. Modeling Supercritical Systems with TOUGH2: Preliminary Results Using the EOS1SC Equation of State, *Twenty-Sixth Workshop on Geothermal Reservoir Engineering*, pp. 2–9. (2001).

Büsing, H., Niederau, J. and Clauser, C. Pressure-enthalpy formulation for numerical simulations of supercritical water/steam systems applied to a reservoir in Tuscany, Italy, *European Geothermal Congress 2016 Strasbourg, France*, pp. 1–6. (2016).

Chen, J. and Jiang, F. Designing multi-well layout for enhanced geothermal system to better exploit hot dry rock geothermal energy, *Renewable Energy*, 74, pp. 37–48. (2015).

Cheng, X., Kuang, B. and Yang, Y. H. Numerical analysis of heat transfer in supercritical water cooled flow channels, *Nuclear Engineering and Design*, 237, pp. 240–252. (2007).

Croucher, A. E. and O'Sullivan, M. J. Application of the computer code TOUGH2 to the simulation of supercritical conditions in geothermal systems, *Geothermics*, 37, pp. 622–634. (2008).

DiPippo, R. Geothermal power plants: Evolution and performance assessments, *Geothermics*, 53, pp. 291–307. (2015).

Duan, C., Zheng, X., Xia, B. and Wang, Z. Temperature Distribution Modeling in Geothermal Wellbore and Formation During the Well Test in Yangyi Geothermal Field , Tibet, *41st Workshop on Geothermal Reservoir Engineering*, pp. 1–8. (2016).

Elders, W. A., Friðleifsson, G. O. and Pálsson, B. Iceland Deep Drilling Project : The first well, IDDP-1, drilled into magma, *Geothermics*, 49, p. 1. (2014).

Elders, W. A., Fridleifsson, G. Ó., Zierenberg, R. A., Pope, E. C., Mortensen, A. K., Gudmundsson, Á., Lowenstern, J. B., Marks, N. E., Owens, L., Bird, D. K., Reed, M., Olsen, N. J. and Schiffman, P. Origin of a rhyolite that intruded a geothermal well while drilling at the Krafla volcano, Iceland, *Geology*, 39(3), pp. 231–234. (2011).

Friðleifsson, G. Ó., Elders, W. A. and Albertsson, A. The concept of the Iceland deep drilling project, *Geothermics*, 49, pp. 2–8. (2014).

Fuss, S., Szolgayova, J., Obersteiner, M. and Gusti, M. Investment under market and climate policy uncertainty, *Applied Energy*, 85, pp. 708–721. (2008).

Hayba, D. O. and Ingebritsen, S. E. The computer model HYDROTHERM a three-dimensional finite-difference model to simulate Ground-Water flow heat transport in the temperature range of 0 to 1 200 °C, *Water-Resources Investigations Report 94-4045*, p. 92. (1994).

Huang, W., Cao, W. and Jiang, F. Heat extraction performance of EGS with heterogeneous reservoir : A numerical evaluation, *International Journal of Heat and Mass Transfer*, 108, pp. 645–657. (2017).

Huang, X., Zhu, J. and Li, J. Analysis of Wellbore Heat Transfer in Enhanced Geothermal System using CFD Modeling, *World Geothermal Congress 2015*, (April), p. 6. (2015a).

Huang, X., Zhu, J. and Li, J. On Wellbore Heat Transfer and Fluid Flow in the Doublet of Enhanced Geothermal System, *Energy Procedia*, 75, pp. 946–955. (2015b).

Ingason, K., Kristjánsson, V. and Einarsson, K. Design and development of the discharge system of IDDP-1, *Geothermics*, 49, pp. 58–65. (2014).

Jiang, F., Luo, L. and Chen, J. A novel three-dimensional transient model for subsurface heat exchange in enhanced geothermal systems, *International Communications in Heat and Mass Transfer*, 41, pp. 57–62. (2013).

Jiang, P., Zhang, L. and Xu, R. Experimental study of convective heat transfer of carbon dioxide at supercritical pressures in a horizontal rock fracture and its application to enhanced geothermal systems, *Applied Thermal Engineering*, 117, pp. 39–49. (2017).

Kissling, W. Extending MULKOM to super-critical temperatures and pressures, *Proceedings of the World Geothermal Congress*, 3, pp. 1687–1690. (1995).

Lenhard, R. and Malcho, M. Numerical simulation device for the transport of geothermal heat with forced circulation of media, *Mathematical and Computer Modelling*, 57(1–2), pp. 111–125. (2013).

Luo, F., Xu, R. N. and Jiang, P. X. Numerical investigation of fluid flow and heat transfer in a doublet enhanced geothermal system with CO2 as the working fluid (CO2-EGS), *Energy*, 64, pp. 307–322. (2014).

Magnusdottir, L. and Finsterle, S. An iTOUGH2 equation-of-state module for modeling supercritical conditions in geothermal reservoirs, *Geothermics*, 57, pp. 8–17. (2015).

Menter, F. R. Zonal two equation k-ω turbulence models for aerodynamic flows, *AIAA 24th Fluid Dynamics Conference, 93-2906*. (1993).

Mortensen, A. K., Egilson, Þ., Gautason, B., Árnadóttir, S. and Guðmundsson, Á. Stratigraphy , alteration mineralogy , permeability and temperature conditions of well IDDP-1 , Krafla , NE-Iceland, *Geothermics*, 49, pp. 31–41. (2014).

Pálsson, B., Hólmgeirsson, S., Guðmundsson, Á., Bóasson, H. Á., Ingason, K., Sverrisson, H. and Thórhallsson, S. Drilling of the well IDDP-1, *Geothermics*, 49, pp. 23–30. (2014).

Pan, L., Freifeld, B., Doughty, C., Zakem, S., Sheu, M., Cutright, B. and Terrall, T. Fully coupled wellbore-reservoir modeling of geothermal heat extraction using CO2 as the working fluid, *Geothermics*, 53, pp. 100–113. (2015).

Pritchett, J. W. STAR : A geothermal reservoir simulation system, *Proceedings World Geothermal Congress Italy*, pp. 2959–2963. (1995).

Scott, S., Driesner, T. and Weis, P. Geologic controls on supercritical geothermal resources above magmatic intrusions, *Nature Communications*. Nature Publishing Group, 6, p. 7837. (2015a).

Scott, S., Driesner, T. and Weis, P. Hydrology of a Supercritical Flow Zone Near a Magmatic Intrusion in the IDDP-1 Well – Insights from Numerical Modeling, *World Geothermal Congress 2015*, 2, p. 5. (2015b).

Suarez Arriaga, M.-C. and Samaniego, F. Deep Geothermal Reservoirs with Fluid at Supercritical Conditions, *Twenty-seventh workshop on geothermal reservoir engineering, Stanford University*. (2013).

Thórhallsson, S., Pálsson, B., Hólmgeirsson, S., Ingason, K. and Matthíasson, M. Well design for the Iceland Deep Drilling Project (IDDP), *Geothermics*, 49, pp. 16–22. (2014).

Vasini, E. M. *Numerical modelling and simulation optimization of geothermal reservoirs using the TOUGH2 family of codes*, *Thesis*. (2016).

Wagner, W., Cooper, J. R., Dittmann, a., Kijima, J., Kretzschmar, H.-J., Kruse, a., Mareš, R., Oguchi, K., Sato, H., Stöcker, I., Šifner, O., Takaishi, Y., Tanishita, I., Trübenbach, J. and Willkommen, T. The IAPWS Industrial Formulation 1997 for the Thermodynamic Properties of Water and Steam, *Journal of Engineering for Gas Turbines and Power*, 122(1), p. 150. (2000).

Wagner, W. and Krezschmar, H.-J. *D2.1 Properties of Water and Steam*. (2010).

Weis, P., Driesner, T., Coumou, D. and Geiger, S. Hydrothermal, multiphase convection of H2O-NaCl fluids from ambient to magmatic temperatures: A new numerical scheme and benchmarks for code comparison, *Geofluids*, 14(3), pp. 347–371. (2014).

CFD modeling of a high enthalpy geothermal context

Renaud, Théo

2018-02-28

Theo Renaud, Michal Stebel, Patrick Verdin and Gioia Falcone. CFD modeling of a high enthalpy geothermal context. Proceedings of the 43rd Workshop on Geothermal Reservoir Engineering, 12-14 Feb 2018, Stanford University, Stanford, California, USA. SGP-TR-213
https://pangea.stanford.edu/ERE/db/GeoConf/papers/SGW/2018/Renaud.pdf